Yanagawa N.

抄読会　Jan, 19, 2024

Article

Patterns of transcription factor programs and immune pathway activation define four major subtypes of SCLC with distinct therapeutic vulnerabilities

Gay CM, Stewart CA, Park EM, et al. Cancer Cell. 2021 Mar 8;39(3):346-360.e7.

肺小細胞癌は肺癌全体の15-20%を占める高悪性度の癌である。形態的にはhomogenous様でありほぼ画一的な治療のみが行われてきたが、近年転写制御因子の発現状態により4つのsubtypeにわけられた。本論文はこのsubtypeと各種治療効果との関連について検討した論文である。

Figure 1：3つの転写制御因子（NeuroD1, POU2F3, ASCL1）の発現状態により、NeuroD1-dominant (SCLC-N), POU2F3-dominant (SCLC-P), ASCL1-dominant (SCLC-A), いずれも低発現 (SCLC-inflamed, SCLC-I)と4つのsubtypeにわかれた。これらは免疫組織化学にて確認可能であった。進行小細胞肺癌をtargetとした治験であるIM power 133においても4つのsubtypeにわけられた。

Figure 3:各subtypeと浸潤免疫担当細胞との関係。SCLC-Iで有意に浸潤細胞数が多い。HeatmapにてもT細胞に関与する18遺伝子の発現がSCLC-I群で他と比べて高い。これはIM power 133でも同様であった。IM power 133はエトポシド+アテゾリツマブ（ICI）とエトポシド＋プラセボを比較した治験であるが、SCLC-P群とSCLC-I群はICI投与群でOSが延長し、SCLC-I群は最も恩恵をうけた。

Figure 4:cell lineを用いた各治療薬の腫瘍増殖抑制効果の検討。SCLC-P群はPARPi, nucleoside analogsなどに感受性を示す一方、SCLC-I, SCLC-N群は抵抗性を示している。

Figure 6:cisplatin投与前と投与後再発したSCLC-A xenograftにおいてASCL1を発現している腫瘍細胞の割合の検討。再発群ではASCL1の割合が低下し、triple negative (SCLC-I)及びEMT score高値の

腫瘍細胞に変わっている。

Take Home Message

・3つの転写制御因子の発現状態により肺小細胞癌は4つのsubtypeにわかれる。

・SCLC-I群はchemo+ICI治療の効果を最も受ける。

・subtypeの変化が治療抵抗性の獲得につながると考えられる。

（査読者　栁川直樹）

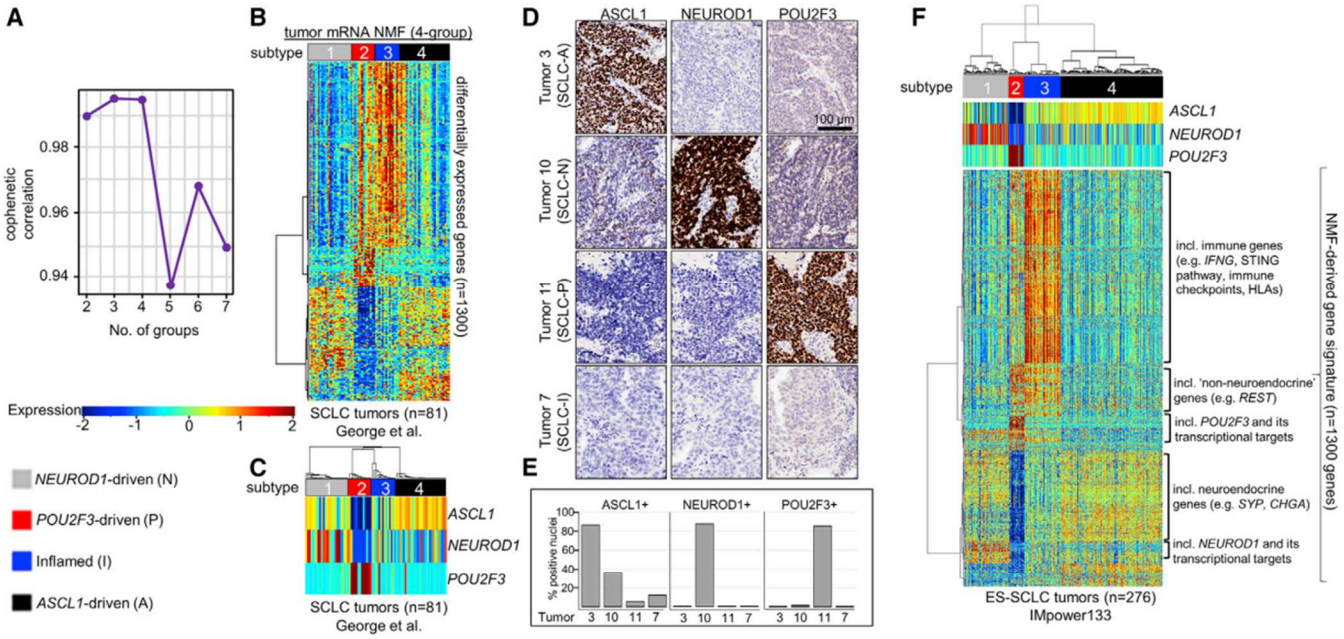

Figure 1. NMF identifies four transcriptional subtypes of SCLC

(A) Cophenetic correlation from NMF analysis of resected SCLC tumors (A).

(B–D) Differential expression of NMF-selected genes (B) and, specifically, *ASCL1, NEUROD1,* and *POU2F3* (C) across 4 clusters. IHC analysis of consecutive sections of patient SCLC tumor for ASCL1, NEUROD1, and POU2F3 demonstrating staining pattern for example of each of four subtypes (D).

(E) Bar graph indicating percentage of tumor cell nuclei positive for ASCL1, NEUROD1, and POU2F3 by IHC in each of four tumors above (E).

(F) Application of NMF-derived gene signature to independent ES-SCLC (IMpower133) tumor dataset revealing four SCLC subtypes (F). Sample sizes: n = 81 tumors (B, C) and n = 276 tumors (F).

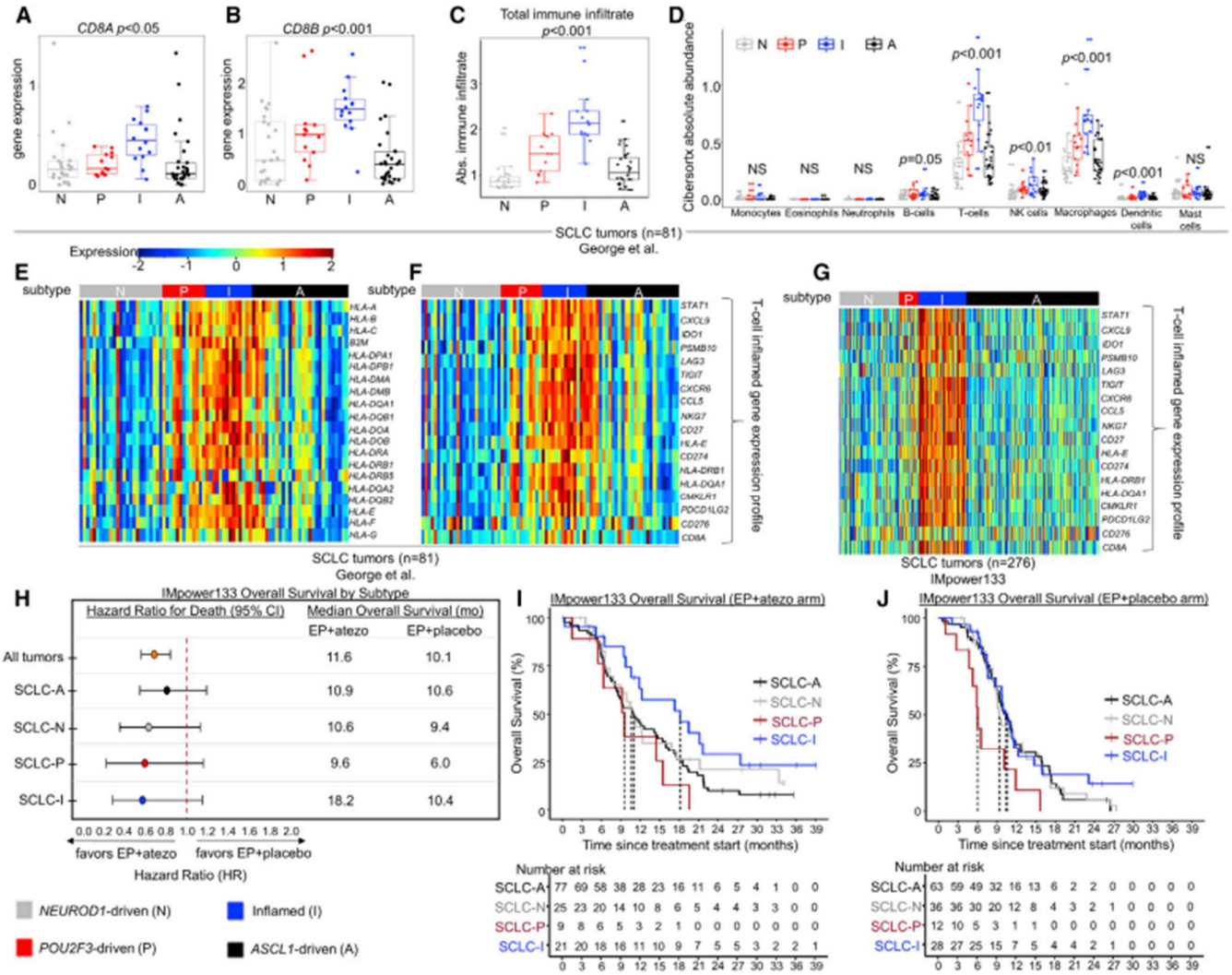

Figure 3. SCLC-I defines an inflamed subtype of SCLC

(A and B) Comparison of mean gene expression of CD8+ T cell markers (A and B).

(C and D) CIBERSORTx analysis of total immune infiltrate (C) and specific immune cell populations (D).

(E and F) Heatmaps comparing expression of HLA and antigen presenting genes (E) and 18-gene -γ-related T cell gene expression profile (F) across subtyped SCLC tumors from George et al.

(G) Heatmap comparing expression of 18-gene -γ-related T cell gene expression profile among tumors from IMpower133 (G).

(H–J) Forest plot demonstrating HRs for OS and median OS values between carboplatin/etoposide + atezolizumab (EP + atezo) and EP + placebo arms in patients from IMpower133 as a collective (all tumors) and by subtype (H). Kaplan-Meier curves on a subtype-by-subtype basis for overall survival in EP + atezo (I) and EP + placebo (J) arms in IMpower133. Sample sizes: n = 81 tumors (A-F), 276 tumors (G), and 132 patients (atezo arm) and 139 patients (placebo arm) (H–J). p values in A–D are the result of one-way ANOVA testing. Error bars: ± 1.5x interquartile range (A–D) and ± 95% CI (H).

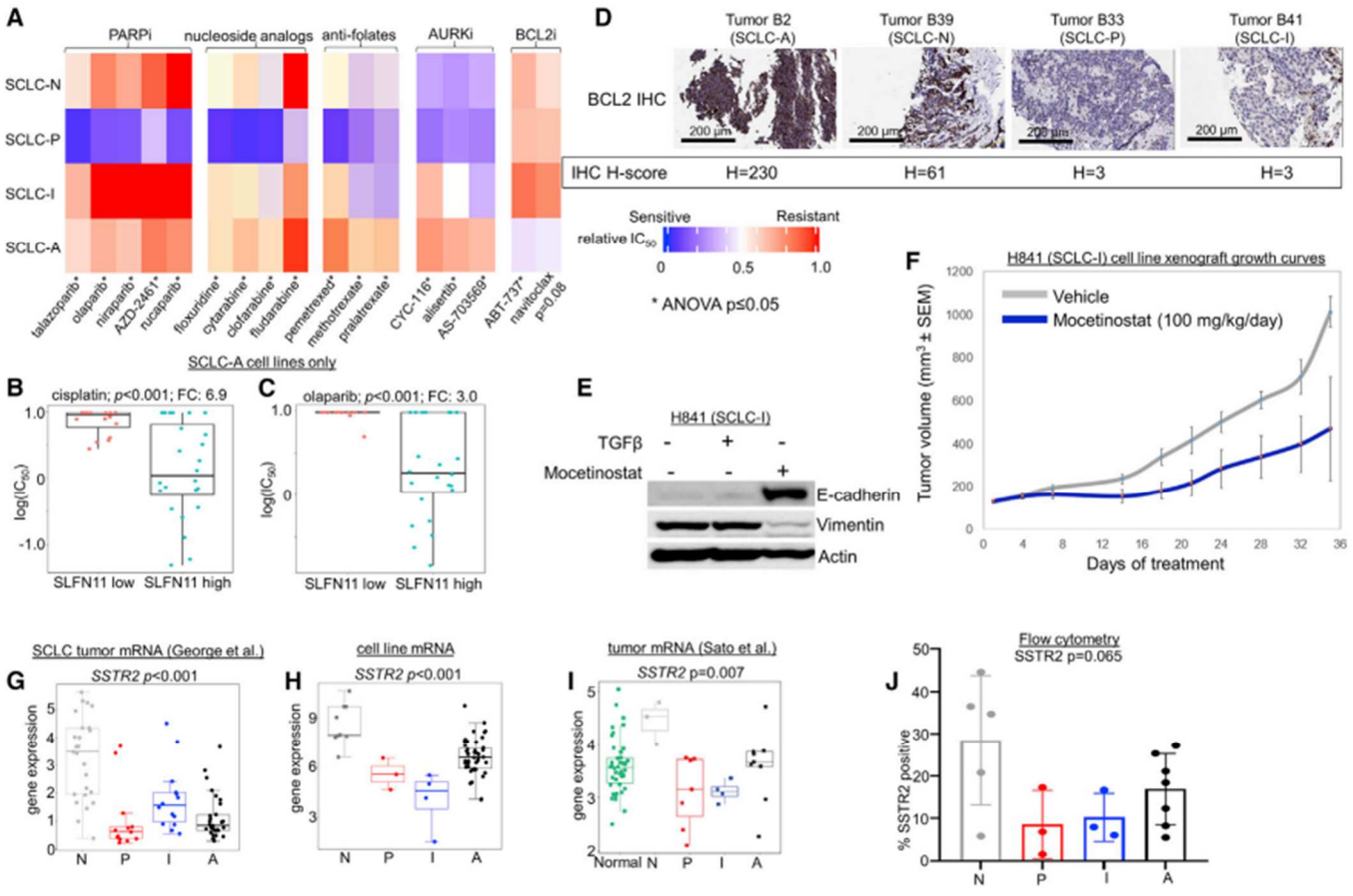

Figure 4. SCLC subtypes possess unique therapeutic vulnerabilities

(A) Comparison between each SCLC cell line subtype of mean relative *in vitro* IC_{50} values for PARP inhibitors, nucleoside analogues, anti-folates, AURK inhibitors, and BCL2 inhibitors (A).

(B and C) Comparison if IC_{50} values for cisplatin (B) and the PARPi olaparib (C) among SCLC-A cell lines separated into high and low SLFN11 expression.

(D) IHC analysis of tumors representing each subtype (representative images for SCLC-A and -N; and n = 1 each for SCLC-P and -I) for expression of BCL2, with associated H-score noted (D).

(E) Western blot showing expression of E-cadherin and Vimentin in H-841 cell line with addition of TGFβ (EMT inducer) and mocetinostat (E).

(F) Murine H841 flank cell line xenograft growth curves with vehicle or mocetinostat treatment (F).

(G–J) Mean expression of the cell surface protein encoding gene *SSTR2* in multiple datasets (G-I) along with flow cytometry analysis of proportion of analyzed cells that express SSTR2 protein in subtyped cell lines (J). Sample sizes: n = 62 cell lines (A, H), n = 38 cell lines (B-C), n = 8 mouse tumors per treatment arm 81 tumors (G), n = 23 tumors (I), and n = 18 cell lines (J). p values are the result of one-way two-sided t test (B-C) or one-way ANOVA (A, G-J). Error bars: ± 1.5x interquartile range (B, C, G–J) or ± SEM (F).

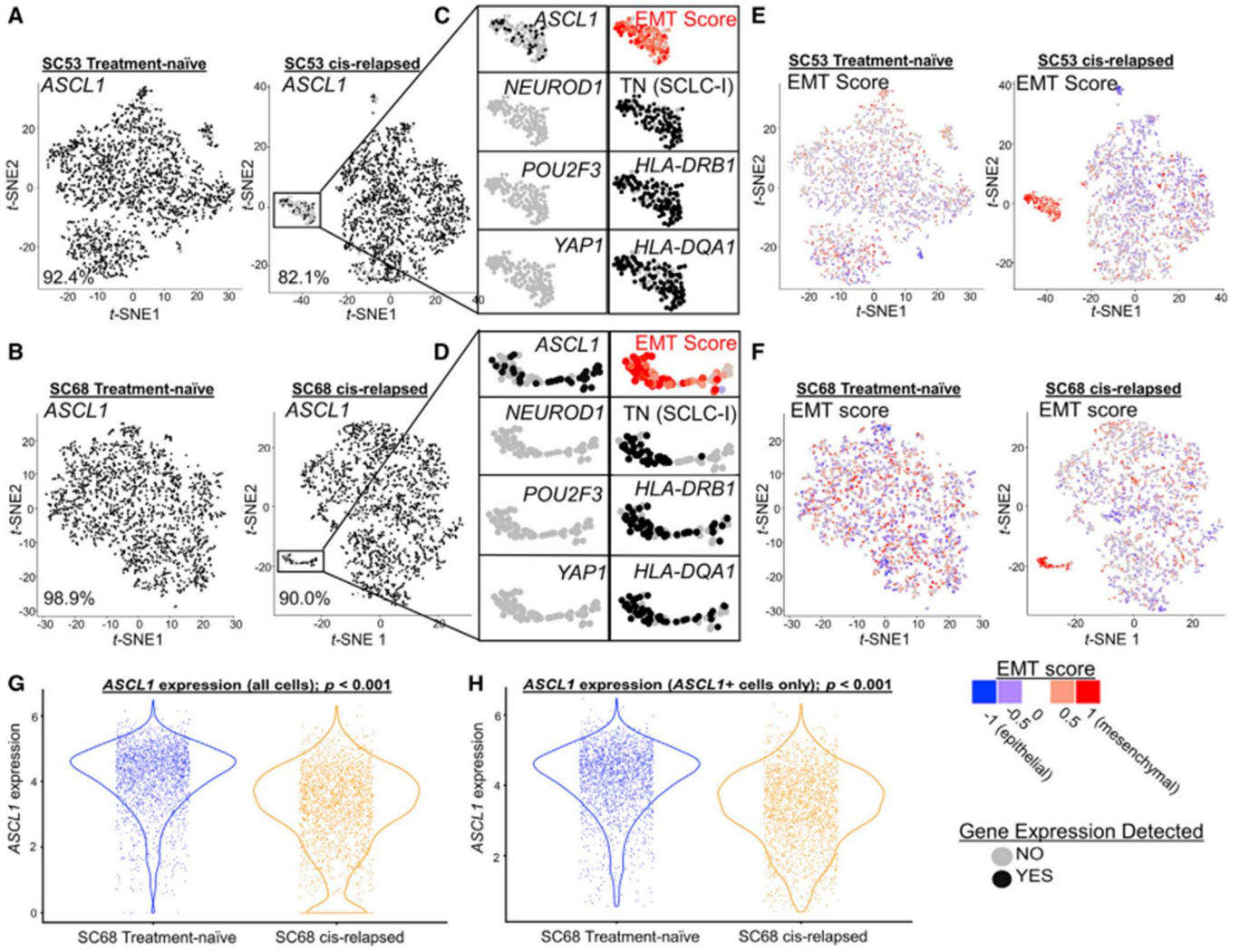

Figure 6. Emergence of SCLC-I populations coincides with cisplatin resistance in SCLC-A predominant xenograft models

(A and B) t-SNE feature plots from scRNAseq for *ASCL1* comparing parental, treatment-naïve, and cisplatin-resistant/relapsed (cis-relapsed) CDX models (MDA-SC53, A; MDA-SC68, B).

(C and D) Highlighted portion of A and B illustrates distinct cluster with prominent *ASCL1* loss (C, D).

(E and F) The cells in this region are now triple-negative (SCLC-I), with high EMT score (E, F).

(G and H) Violin plots comparing *ASCL1* expression between MDA-SC68 treatment-naïve and cisplatin-relapsed xenograft tumors in all cells (G) and only *ASCL1*-positive cells (H). Sample sizes: n = 2000 cells per arm (A–H). p values are the result of two-tailed t test (G, H).